Density-functional theory of the water liquid-vapour interface: II

1994 J. Phys.: Condens. Matter 6 4823

(http://iopscience.iop.org/0953-8984/6/26/005)

J. Phys.: Condens. Matter 6 (1994) 4823–4842. Printed in the UK

Density-functional theory of the water liquid–vapour interface: II

B Yang, D E Sullivan and C G Gray

Guelph-Waterloo Program for Graduate Work in Physics, University of Guelph, Guelph, Ontario, Canada N1G 2W1

Received 5 January 1994, in final form 18 March 1994

Abstract. An improvement of our previous extended mean-field theory of the liquid–vapour interface of water is described. This revision extends the range of validity of the theory to room temperature. The current theory is improved in three aspects: (1) the effective angle-averaged pair potential is obtained by the RAM (reference-averaged Mayer) function approximation, avoiding expansion in inverse powers of temperature; (2) the soft repulsive core of the TIP4P water model pair potential is treated accurately; and (3) the anisotropic interactions are represented by a higher-order ($l = 5$) multipole expansion. The current theory includes no adjustable parameters; the critical temperature T_c is found to be 609 K. Detailed calculations are given for room temperature, where molecular-dynamics simulation results are available for comparison. A more detailed representation of the orientational distribution function is reported.

1. Introduction

In recent years, density-functional methods have been widely applied, with significant success, to the study of classical inhomogeneous fluids [1]. Most of these applications have been to models of simple, i.e., monatomic fluids. Progress in the development of density-functional theories for molecular fluids has been slower, as is understandable due to the increased complexity of such systems. Nonetheless, there have been several works on this subject, with application to bulk phase transitions and interfacial properties of liquid crystals [2–4], amphiphile solutions [5], Langmuir monolayers [6], polar liquids [7–11], and other molecular fluids [12, 13].

The present article involves re-examining density-functional theory for the specific case of the liquid–vapour interface of water. The theory described here should also be applicable to other fluids composed of strongly polar molecules, albeit ones restricted to exhibiting weak anisotropy of the repulsive molecular cores. Here we are concerned with revising an earlier theory of ours [8], which in turn was motivated by a theory of the liquid–vapour interface of polar fluids proposed by Teixeira and Telo da Gama [7]. Underlying these earlier theories was an expansion of the grand canonical potential in powers of the anisotropic (multipolar) part of the intermolecular pair potential. This effectively amounts to a high-temperature perturbation expansion. When applied to a model pair potential (namely TIP4P [14, 15]) characterizing water, the theory was found [8] to produce an unstable bulk liquid phase at temperatures below about 400 K, clearly a consequence of the underlying perturbation expansion. In this paper we examine a revised theory closely related to that of [7, 8] but avoiding the expansion in powers of the potential. For the same model of water as before, the present theory yields stable solutions over the whole physical temperature

0953-8984/94/264823+20$19.50

range of liquid water. The approach used here may be termed an amalgam of mean-field theory with a generalized version (i.e., applicable to inhomogeneous fluids) of the 'reference-averaged Mayer (RAM) function' theory [16]. The detailed description of the theory and significant technical aspects involved in its numerical implementation are given in section 2.

As in [8], we apply the theory to the analysis of orientational ordering at the liquid–vapour interface of water, focusing on the behaviour near room temperature which was inaccessible in our earlier work. Nonetheless, the results are qualitatively similar to those obtained in [8]. This is discussed in section 3. Here we describe a more detailed representation of the interfacial ordering than that given in [8], in particular, based on three-dimensional plots of the orientational probability density as a function of its relevant Euler angles. This shows that there are significant variations in orientational structure with distance through the interface. However, the most statistically significant structures are those occurring near the high-density, bulk liquid edge of the interface, which are dominated by alignment of molecules with their dipole axes parallel and HOH planes perpendicular to the interfacial plane. This ordering is accompanied by a weak asymmetry in the distribution of dipole axes, resulting in a net inclination of molecular dipoles toward the bulk liquid phase. These results are consistent with those of recent computer simulations, principally the work of Wilson *et al* [15], although differences are found in the nature of ordering near the low-density, vapour edge of the interface. The comparison with simulation results also indicates that the present theory may quantitatively underestimate the degree of interfacial orientational ordering. Possible reasons for this discrepancy, as well as further discussion of our findings and conclusions, are contained in the final section 4, of the paper.

2. Theory

2.1. The free energy functional

We recapitulate the basic mean-field equations for a classical inhomogeneous molecular fluid [2–11]. The molecular degrees of freedom, i.e., position $\boldsymbol{r}$ and orientational Euler angles ω, will be collectively denoted by the symbol x. We assume the intermolecular pair potential $V(x_1, x_2)$ has the form

$$V(x_1, x_2) = V_{\text{ref}}(r_{12}) + V_{\text{pert}}(x_1, x_2) \tag{1}$$

where $V_{\text{ref}}(r_{12})$ is an isotropic reference potential depending only on the intermolecular distance $r_{12} \equiv |r_2 - r_1|$. Our further development assumes that $V_{\text{ref}}(r_{12})$ contains *all* the short-range repulsive contributions to the pair potential, and *no other* contributions. All remaining pair interactions, including all anisotropic effects plus 'long-range' isotropic attractions, are contained in $V_{\text{pert}}(x_1, x_2)$. We separate the latter contributions by further writing

$$V_{\text{pert}}(x_1, x_2) = V_{\text{att}}(r_{12}) + V_{\text{an}}(x_1, x_2). \tag{2}$$

Now, in the absence of external fields, the mean-field approximation for the grand canonical variational potential Ω is

$$\Omega = \int \mathrm{d}\boldsymbol{r}\, f_{\text{ref}}(\rho(r)) + \int \mathrm{d}x\, \rho(x)[kT \ln(8\pi^2 f(x)) - \mu_c] + \Delta\Omega_{\text{MF}} \tag{3}$$

$$\Delta\Omega_{\text{MF}} = \tfrac{1}{2} \int \mathrm{d}x_1\, \mathrm{d}x_2\, \rho(x_1) V_{\text{pert}}(x_1, x_2) \rho(x_2). \tag{4}$$

Here μ_c is the chemical potential, $\rho(x)$ is the one-particle probability density, $\rho(r) \equiv \int d\omega\, \rho(x)$ is the angle-averaged number density, and $f(x) \equiv \rho(x)/\rho(r)$ is the normalized orientational distribution function; $\int dx_i$ denotes $\int dr_i \int d\omega_i$. In (3), the contribution of the repulsive potential V_{ref} to the grand potential has been treated in a local thermodynamic approximation, where $f_{ref}(\rho)$ is the Helmholtz free-energy density of a uniform bulk fluid of number density ρ interacting via pair potential $V_{ref}(r_{12})$. More refined treatments of the repulsive force contribution, based on 'weighted-density' techniques (see, e.g., [3]), are available but will not be considered in this work.

Consider the decomposition of $V_{pert}(x_1, x_2)$ in (2). As discussed in [8], in those cases where the unweighted angle averages of $V_{an}(x_1, x_2)$ (over either or both of ω_1, ω_2) vanish, this interaction makes no contribution to the equilibrium grand potential Ω_{eq} obtained by minimizing (3) with respect to $\rho(x)$. This deficiency led Teixeira and Telo da Gama [7] to replace $\Delta\Omega_{MF}$ in (4) by the following generalized mean-field functional $\Delta\Omega_{GMF}$:

$$\Delta\Omega_{GMF} = \tfrac{1}{2}\int dx_1\, dx_2\, \rho(x_1)\rho(x_2)\left[V_{pert}(x_1, x_2) - \frac{\beta}{2}V_{pert}^2(x_1, x_2)\right] \tag{5}$$

where $\beta = 1/kT$. In their original derivation, this formula was obtained from an expression containing $[1 - \exp(-\beta V_{pert})]$ in the integral. The theory described by the present authors in [8], derived by a quite different route, yielded a generalized functional similar to that of (5) but containing additional terms of quadratic order in $V_{pert}(x_1, x_2)$. One effect of these additional terms was that the isotropic attraction $V_{att}(r_{12})$ cancelled out from all quadratic terms and thus contributed only to linear, 'mean-field', order. However, the quantitative effect of the additional terms (after removing $V_{att}(r_{12})$) appears to be minimal, so that for practical purposes the theory of [8] is equivalent to using $\Delta\Omega_{GMF}$ as given by (5), with $V_{pert}^2(x_1, x_2)$ replaced by $V_{an}^2(x_1, x_2)$.

The present proposed revision of the theory can be motivated by rewriting the original mean-field expression (4) using the factorization $\rho(x) = \rho(r)f(x)$:

$$\Delta\Omega_{MF} = \tfrac{1}{2}\int dr_1\, dr_2\, \rho(r_1)\bar{V}_{pert}(r_1, r_2)\rho(r_2) \tag{6}$$

where

$$\bar{V}_{pert}(r_1, r_2) = \int d\omega_1\, d\omega_2\, f(x_1)V_{pert}(x_1, x_2)f(x_2). \tag{7}$$

In this form, the contribution of all anisotropic forces to the grand potential is equivalent to that of a fluid interacting by an effective orientation-independent potential $\bar{V}_{pert}(r_1, r_2)$. This picture of replacing the actual anisotropic fluid by an angle-independent reference fluid underlies most perturbation theories of bulk isotropic phases in such fluids [17, 18], where $f(x)$ is constant. For an inhomogeneous fluid, $f(x)$ is generally constant with respect to neither position nor orientation, and the effective potential defined by (7) is functionally dependent (via $f(x)$) on the spatial inhomogeneity and orientational order [19]. From this viewpoint, the expression (7) is equivalent to the most rudimentary form of molecular perturbation theory, based on direct linear averaging of the anisotropic potential. Several other fairly simple prescriptions for obtaining the effective angle-averaged potential have been developed [18], but here we consider only the best known of these, based on averaging the Boltzmann factor of the potential [19]:

$$e^{-\beta\bar{V}_{pert}(r_1, r_2)} = \int d\omega_1\, d\omega_2\, f(x_1)f(x_2)e^{-\beta V_{pert}(x_1, x_2)}. \tag{8}$$

For a uniform isotropic fluid, this reduces to the prescription of RAM perturbation theory [16–19]. On substituting (2), the isotropic component $V_{\rm att}(r_{12})$ is unaffected by the angle averaging, and hence

$$\bar{V}_{\rm pert}(\boldsymbol{r}_1, \boldsymbol{r}_2) = V_{\rm att}(r_{12}) + \bar{V}_{an}(\boldsymbol{r}_1, \boldsymbol{r}_2) \tag{9}$$

where

$$\mathrm{e}^{-\beta \bar{V}_{\rm an}(\boldsymbol{r}_1,\boldsymbol{r}_2)} = \int \mathrm{d}\omega_1\, \mathrm{d}\omega_2\, f(\boldsymbol{x}_1) f(\boldsymbol{x}_2) \mathrm{e}^{-\beta V_{\rm an}(\boldsymbol{x}_1,\boldsymbol{x}_2)}. \tag{10}$$

Solving the latter by expansion in powers of β gives

$$\bar{V}_{\rm an}(\boldsymbol{r}_1, \boldsymbol{r}_2) = \int \mathrm{d}\omega_1\, \mathrm{d}\omega_2\, f(\boldsymbol{x}_1) f(\boldsymbol{x}_2) \left[V_{\rm an}(\boldsymbol{x}_1, \boldsymbol{x}_2) - \frac{\beta}{2} V_{\rm an}^2(\boldsymbol{x}_1, \boldsymbol{x}_2) \right]$$
$$+ \frac{\beta}{2} \left[\int \mathrm{d}\omega_1\, \mathrm{d}\omega_2\, f(\boldsymbol{x}_1) f(\boldsymbol{x}_2) V_{\rm an}(\boldsymbol{x}_1, \boldsymbol{x}_2) \right]^2 + \mathrm{O}(\beta^2). \tag{11}$$

This is similar to the approximation used in [8] (see equations (7) and (8) in [8]) but differs slightly in the terms corresponding to the second line of (11). In this paper, we will retain the unexpanded expression in (10).

We introduce one further modification, namely to generalize (6) by including the correlation function $g_{\rm ref}(\boldsymbol{r}_1, \boldsymbol{r}_2)$ of the reference repulsive fluid:

$$\Delta\Omega_{MF} = \tfrac{1}{2} \int \mathrm{d}\boldsymbol{r}_1\, \mathrm{d}\boldsymbol{r}_2\, g_{\rm ref}(\boldsymbol{r}_1, \boldsymbol{r}_2) \rho(\boldsymbol{r}_1) \rho(\boldsymbol{r}_2) \bar{V}_{\rm pert}(\boldsymbol{r}_1, \boldsymbol{r}_2). \tag{12}$$

This inclusion of $g_{\rm ref}(\boldsymbol{r}_1, \boldsymbol{r}_2)$ can be expected on general grounds [7, 10]. While ultimately it would be desirable to consider an approximation for $g_{\rm ref}(\boldsymbol{r}_1, \boldsymbol{r}_2)$ embodying features of a high-density, inhomogeneous fluid, here we limit ourselves to the low-density approximation [7]

$$g_{\rm ref}(\boldsymbol{r}_1, \boldsymbol{r}_2) = \mathrm{e}^{-\beta V_{\rm ref}(r_{12})}. \tag{13}$$

Since $V_{\rm ref}(r_{12})$ is taken to be an isotropic repulsive potential, effectively the function $g_{\rm ref}$ does no more than provide a smooth cut-off to $\bar{V}_{\rm pert}(\boldsymbol{r}_1, \boldsymbol{r}_2)$ in (12) at distance r_{12} within the repulsive core. The ambiguity in otherwise treating the small-r_{12} limit of $\bar{V}_{\rm pert}(\boldsymbol{r}_1, \boldsymbol{r}_2)$ is our main motivation for the introduction of $g_{\rm ref}(\boldsymbol{r}_1, \boldsymbol{r}_2)$.

In summary, our approximate free-energy functional Ω is given by equations (3), (9), (10), (12), and (13). The equilibrium grand canonical potential $\Omega_{\rm eq}$ is the minimum of Ω on variation with respect to the probability density $\rho(\boldsymbol{x})$. The condition $\delta\Omega/\delta\rho(\boldsymbol{x}) = 0$ can be separated into two coupled relations [2]

$$\frac{\delta\Omega}{\delta\rho(\boldsymbol{r})} = 0 \qquad \text{(fixed } f(\boldsymbol{x})\text{)} \tag{14}$$

$$\frac{\delta\Omega}{\delta f(\boldsymbol{x})} = \lambda(\boldsymbol{r}) \qquad \text{(fixed } \rho(\boldsymbol{r})\text{)} \tag{15}$$

where $\lambda(r)$ in (15) is a Lagrange multiplier introduced to satisfy the normalization condition $\int \mathrm{d}w f(x) = 1$. These conditions yield the following coupled equations for the equilibrium orientational distribution function and number density:

$$f(x) = \frac{\mathrm{e}^{-\beta\Phi(x)}}{\int \mathrm{d}w\, \mathrm{e}^{-\beta\Phi(x)}} \tag{16}$$

where

$$\Phi(x_1) = -kT \int \mathrm{d}x_2\, \rho(r_2) f(x_2) \mathrm{e}^{-\beta V_{\mathrm{ref}}(r_{12})} \mathrm{e}^{\beta \bar{V}_{\mathrm{an}}(r_1, r_2)} [\mathrm{e}^{-\beta V_{\mathrm{an}}(x_1, x_2)} - 1] \tag{17}$$

and

$$\mu_c = \mu_{\mathrm{ref}}(\rho(r_1)) + kT \int \mathrm{d}w_1\, f(x_1) \ln(8\pi^2 f(x_1)) + \int \mathrm{d}r_2\, \rho(r_2) \mathrm{e}^{-\beta V_{\mathrm{ref}}(r_{12})} [V_{\mathrm{att}}(r_{12}) + \bar{V}_{\mathrm{an}}(r_1, r_2)]. \tag{18}$$

In the last equation, $\mu_{\mathrm{ref}} = \partial f_{\mathrm{ref}}/\partial\rho$ is the chemical potential of the repulsive reference fluid.

For a bulk disordered fluid, the approximate free energy derived here agrees with a combined RAM–mean-field theory applied by Woodward and Nordholm to the dipolar hard-sphere model [20]. Later work by these authors [21] extended their theory to non-uniform fluids by means of a 'constrained RAM' (CRAM) theory, which, however, is not equivalent to the present theory but includes orientational correlations in a more complicated manner (essentially equivalent to the Bethe or two-particle cluster approximation of lattice systems). Another treatment, similar to ours, but restricted to dipolar fluids and therefore not applicable to water, has recently been described by Frodl and Dietrich [10, 11]; it is equivalent to the original, unexpanded form of the theory developed by Teixeira and Telo da Gama [7]. The work in [11] contains a detailed comparison of different theoretical treatments for bulk and interfacial properties of the Stockmayer model of dipolar fluids.

In this paper we apply the theory to the TIP4P [14] model of water. In this case, the total pair potential $V(x_1, x_2)$ is a sum of site–site interactions, consisting of a single Lennard-Jones term $V_{\mathrm{LJ}}(r_{12})$ acting between the water oxygen nuclei plus Coulomb interactions between all intermolecular pairs of charges. It is the latter electrostatic interaction which constitutes the anisotropic potential $V_{\mathrm{an}}(x_1, x_2)$. In [8], this was approximated by its leading-order dipolar and quadrupolar terms, while in this work we use a higher-order multipole expansion of $V_{\mathrm{an}}(x_1, x_2)$ (see below). The Lennard-Jones potential $V_{\mathrm{LJ}}(r_{12})$ is separated into repulsive (V_{ref}) and attractive (V_{att}) components using the Weeks–Chandler–Andersen (WCA) prescription [22]. Following WCA, the thermodynamic functions of the reference repulsive fluid are approximated by those of a hard-sphere fluid with density- and temperature-dependent diameter $d = d(\rho, T)$. The Carnahan–Starling approximation is used for the reference free-energy density $f_{\mathrm{ref}}(\rho)$.

2.2. *The expansion of the angular functions*

The coupled equations (16)–(18) are solved for a planar liquid–vapour interface using a conventional iterative technique [8]. The z-axis is taken to be normal to the interface, with positive direction pointing from liquid to vapour. Then $\rho(r) = \rho(z)$ and $f(x) = f(z, \omega)$.

Due to azimuthal symmetry in directions parallel to the interface, the ω-dependence of $f(z,\omega)$ only involves the polar angle θ and dihedral angle χ, defined in figure 1 of [8].

The expressions that involve angular variables are generally very complicated. To facilitate the computation, we expand all functions of orientations in terms of generalized spherical harmonics $D^l_{mn}(\omega)$ [17]:

$$f(z,\omega) = \sum_{ln} f_{ln}(z) D^l_{0n}(\omega) \tag{19}$$

$$\beta\Phi(z,\omega) = \sum_{ln} \Phi_{ln}(z) D^l_{0n}(\omega) \tag{20}$$

$$F(r_{12},\omega_1,\omega_2) \equiv e^{-\beta V_{nn}(x_1,x_2)} - 1 = \sum_{l_1 l_2 l} \sum_{\substack{m_1 m_2 m \\ n_1 n_2}} F(l_1,l_2,l,n_1,n_2;r_{12}) C(l_1,l_2,l;m_1,m_2,m) \times D^{l_1}_{m_1 n_1}(\omega_1)^* D^{l_2}_{m_2 n_2}(\omega_2)^* Y_{lm}(\omega_{12})^* \tag{21}$$

where ω_{12} denotes the orientation of the intermolecular vector $r_{12} \equiv r_2 - r_1$, $C(l_1,l_2,l;m_1,m_2,m)$ is a Clebsch–Gordan coefficient, and $Y_{lm}(\omega_{12})$ is a spherical harmonic. The coefficients $F(l_1,l_2,l,n_1,n_2;r_{12})$ can be evaluated by using the orthogonality properties of $D^{l_1}_{m_1 n_1}(\omega)$, $Y_{lm}(\omega_{12})$, and $C(l_1,l_2,l;m_1,m_2,m)$ (see subsection 2.3 for details).

It follows from the the above definitions and (10) and (17) that

$$\begin{aligned}\Phi_{l_1 n_1}(z) = -2\pi \sum_{l_2,n_2 l} \int_{-\infty}^{\infty} \frac{\rho(z+z_{12}) f_{l_2 n_2}(z+z_{12})}{2l_2+1} dz_{12} \int_{|z_{12}|}^{\infty} r_{12}\, dr_{12} \\ \times 8\pi^2 F(l_1,l_2,l,n_1,n_2;r_{12}) C(l_1,l_2,l;0,0,0) Y_{l0}(\omega_{12})^* \\ \times \Bigg[1 + \sum_{\substack{l_1' n_1' \\ l_2' n_2' \\ l'}} \frac{(8\pi^2)^2 f_{l_1' n_1'}(z) f_{l_2' n_2'}(z+z_{12})}{(2l_1'+1)(2l_2'+1)} F(l_1',l_2',l',n_1',n_2';r_{12}) \\ \times C(l_1',l_2',l';0,0,0) Y_{l'0}(\omega_{12})^* \Bigg]^{-1}.\end{aligned} \tag{22}$$

So far, there are no mathematical approximations. In practice, the iterative solution of these equations is extremely time consuming, mainly due to the fact that the iteration variables $f_{ln}(z)$ are involved in the integral $\int dr_{12}[\ldots]$ in (22). Therefore approximations must be made such that $f_{ln}(z)$ can be factored out of the integral $\int dr_{12}[\ldots]$. Assuming that the liquid–vapour interfacial orientational ordering is weak, namely that $f_{ln}(z)$ $(l \neq 0)$ is small compared to f_{00}, one can expand the integrand of (22) to first order in f_{ln}/f_{00}. After the expansion, we have

$$\begin{aligned}\Phi_{l_1 n_1}(z) = \int \rho(z+z_{12})\, dz_{12} \Bigg\{ -\sum_{l_2 n_2 l} f_{l_2 n_2}(z+z_{12}) \int_{|z_{12}|}^{\infty} r_{12}\, dr_{12}\, 8\pi^2 \frac{\sqrt{\pi(2l+1)}}{2l_2+1} \\ \times G(l_1,l_2,l,n_1,n_2;r_{12}) C(l_1,l_2,l;0,0,0) P_l\left(\frac{z_{12}}{r_{12}}\right) \\ + \sum_{\substack{l_2 n_2 \\ l_2 \neq 0}} (f_{l_2 n_2}(z) + (-1)^{l_2} f_{l_2 n_2}(z+z_{12})) \int r_{12}\, dr_{12}\, 4\pi^2 \sqrt{\frac{2l_1+1}{2l_2+1}} \\ \times G(l_1,0,l_1,n_1,0;r_{12}) G(l_2,0,l_2,n_2,0;r_{12}) P_{l_1}\left(\frac{z_{12}}{r_{12}}\right) P_{l_2}\left(\frac{z_{12}}{r_{12}}\right) \Bigg\}\end{aligned} \tag{23}$$

where

$$G(l_1, l_2, l, n_1, n_2; r_{12}) = \frac{F(l_1, l_2, l, n_1, n_2; r_{12})}{1 + (1/\sqrt{4\pi})F(0, 0, 0, 0, 0; r_{12})}$$

and P_l denotes a Legendre polynomial. Now given the functions $G(l_1, l_2, l, n_1, n_2; r_{12})$, the integrals over r_{12} above can be computed once and for all for each temperature. The same type of expansion is used for evaluating $\bar{V}_{an}(r_1, r_2)$ in (18).

Another approximation has to be made for the computation to be feasible in practice, since the sums contain an infinite number of terms. Numerically, it is neither necessary nor feasible to keep all of them. In this paper, we choose to use maximum $l = 5$ for all spherical harmonic indices. We mention that a spherical harmonic expansion of the TIP4P electrostatic potential $V_{an}(x_1, x_2)$ (which is a pure multipolar expansion) with $l_{max} = 5$ yielded a very accurate representation of this interaction energy. Also, from our results we find $f_{5n}(z)$ to be much smaller than the leading order parameters, hence the choice $l_{max} = 5$ is appropriate and accurate for all practical purposes.

The solution of these equations proceeds by iteration between equation (16) and equations (20) and (23), i.e., using the result of the latter pair of equations (with some input functions $f_{ln}(z)$ and $\rho(z)$) to evaluate $f(z, \omega)$ from equation (16). A new set of functions $f_{ln}(z)$ is then generated from the inverse of equation (19)

$$f_{ln}(z) = \frac{2l+1}{8\pi^2} \int d\omega \, D^l_{on}(\omega)^* f(z, \omega). \tag{24}$$

The density profile $\rho(z)$ is recomputed by adjusting $\rho(z)$ in $\mu_{ref}(\rho(z))$ in (18) such that the condition $\mu_c = \mu_{c,bulk}$ remains valid for all z.

2.3. The calculation of the rotational invariants $F(l_1, l_2, l, n_1, n_2; r_{12})$

The main stumbling block for the computation is the calculation of the expansion coefficients $F(l_1, l_2, l, n_1, n_2; r_{12})$ of $e^{-\beta V_{an}}$. The binary expansion and extrapolation method given by Fries and Patey [23] works well at large molecular separation but fails significantly at short separations, where it matters most for the interfacial problem since the water liquid–vapour interfacial thickness is only about two molecular diameters. We have instead resorted to a direct integral evaluation of these coefficients, which involves five-dimensional angular integration. The symmetry properties of the interaction $V_{an}(x_1, x_2)$ must be fully exploited to make such a calculation feasible.

We choose an axial frame in which molecule 1 is fixed in orientation, i.e., $\omega_1 = 0$. Then $D^{l_1}_{m_1,n_1}(\omega_1) = \delta_{m_1 n_1}$, and $F(l_1, l_2, l, n_1, n_2; r_{12})$ is obtained from the relation

$$F(l_1, l_2, l, n_1, n_2; r_{12}) = \frac{(2l_1+1)(2l_2+1)}{8\pi^2(2l+1)} \sum_{m_2} C(l_1, l_2, l; n_1, m_2, m)$$
$$\times \int d\omega_2 \, d\omega_{12} \, (e^{-\beta V_{an}(x_1, x_2)} - 1) D^{l_2}_{m_2 n_2}(\omega_2) Y_{lm}(\omega_{12}) \tag{25}$$

where $m = n_1 + m_2$. In the same axial frame, the multipole expansion of $V_{an}(x_1, x_2)$ is given by

$$V_{an}(x_1, x_2) = \sum_{l_1 l_2} \frac{A_{l_1 l_2}}{r_{12}^{l_1+l_2+1}} \sum_{m_1 m_2} C(l_1, l_2, l; m_1, m_2, m) Y_{lm}(\omega_{12})^* \sum_{n_2} Q_{l_1 m_1} Q_{l_2 n_2} D^{l_2}_{m_2 n_2}(\omega_2)^* \tag{26}$$

where $l = l_1 + l_2$ and $A_{l_1 l_2}$ and the spherical multipole moments Q_{ln} are defined in equations (2.169) and (2.74) in [17], respectively. We have used the latter formula to calculate the required Q_{ln} from the TIP4P point charge distribution for the water molecule.

To optimize the five-dimensional integral in (25), we regroup the factors in (26) in order to minimize the number of different angular functions involved in the summations. We also use the fact that only even-n moments Q_{ln} are non-zero for the C_{2v} symmetry of water, with $Q_{l\underline{n}} = Q_{ln}$, where $\underline{n} = -n$. Then (26) can be written as

$$V_{\mathrm{an}}(x_1, x_2) = \sum_{l_1 l_2} \frac{A_{l_1 l_2}}{r_{12}^{l_1+l_2+1}} \sum_{m_1=0}^{l_1} \tilde{Q}_{l_1 m_1} \times \sum_{m_2=0}^{l_2} [C'(l_1, l_2, l; m_1, m_2, m_1 + m_2)\,\mathrm{Re}(Y_{lm_1+m_2}(\omega_{12}) S_{l_2 m_2}(\omega_2)) + C'(l_1, l_2, l; m_1, \underline{m_2}, m_1 + \underline{m_2})\,\mathrm{Re}(Y_{lm_1+\underline{m_2}}(\omega_{12}) S^*_{l_2 m_2}(\omega_2))] \tag{27}$$

where

$$C'(l_1, l_2, l; m_1, m_2, m) = \begin{cases} 2C(l_1, l_2, l; m_1, m_2, m) & \text{if } m_2 > 0 \\ C(l_1, l_2, l; m_1, m_2, m) & \text{if } m_2 = 0 \\ (-)^{m_2} 2C(l_1, l_2, l; m_1, m_2, m) & \text{if } m_2 < 0 \end{cases}$$

$$\tilde{Q}_{l_1 m_1} = \begin{cases} Q_{l_1 m_1} & \text{if } m_1 \neq 0 \\ \frac{1}{2} Q_{l_1 0} & \text{if } m_1 = 0 \end{cases}$$

and

$$S_{l_2 m_2}(\omega_2) = \sum_{n_2=0}^{l_2} \tilde{Q}_{l_2 n_2} (D^{l_2}_{m_2 n_2}(\omega_2) + D^{l_2}_{m_2 \underline{n_2}}(\omega_2)).$$

We use the following order of integration in (25), from innermost to outermost: $\phi_{12}, \theta_{12}, \chi_2, \phi_2, \theta_2$. Thus in the innermost integration loop (over ϕ_{12}), most of the angular functions (e.g., S_{lm}) in $V_{\mathrm{an}}(x_1, x_2)$ do not need to be evaluated repeatedly. It is also very important to factorize all spherical harmonics $Y_{lm}(\omega_{12})$ and $D^{l_2}_{m_2 n_2}(\omega_2)$ into products of separate angular functions, leaving only the absolutely minimal computation present in the innermost loop.

The angular integrations in (25) were done using Gaussian quadrature in all five dimensions; 20-point Gaussian quadrature yielded results with less than 1% error compared to 30 or more points. With these prescriptions, the computation time for $F(l_1, l_2, l, n_1, n_2; r_{12})$ at a single r_{12} value was cut down from almost a month to less than 1 min on a Silicon Graphics 4D35.

3. Results

As remarked earlier, all interaction parameters are computed for the TIP4P site-site potential model. In contrast with our earlier work [8], which replaced the soft LJ core of the TIP4P model by a hard-sphere core with fixed diameter treated as an adjustable parameter, there

are no adjustable parameters in the present calculations. We first show in figure 1 the bulk liquid–vapour coexistence curve predicted by the theory, in comparison with both the experimental curve for water [24] and available computer simulation results for the TIP4P model [25]. The theoretical critical temperature T_c and density ρ_c are found to be 609 K and 0.277 g cm^{-3}, to be compared with experimental values of 647 K and 0.322 g cm^{-3}, respectively. Overall, the theory agrees reasonably well with experiment and simulation, the major discrepancy being in the shape of the liquidus curve at high temperatures. As well, below room temperature, the predicted liquid densities overshoot the experimental values: at $T = 300$ K, the theory predicts the liquid density to be 1.047 g cm^{-3}, compared with 0.997 g cm^{-3} from experiment.

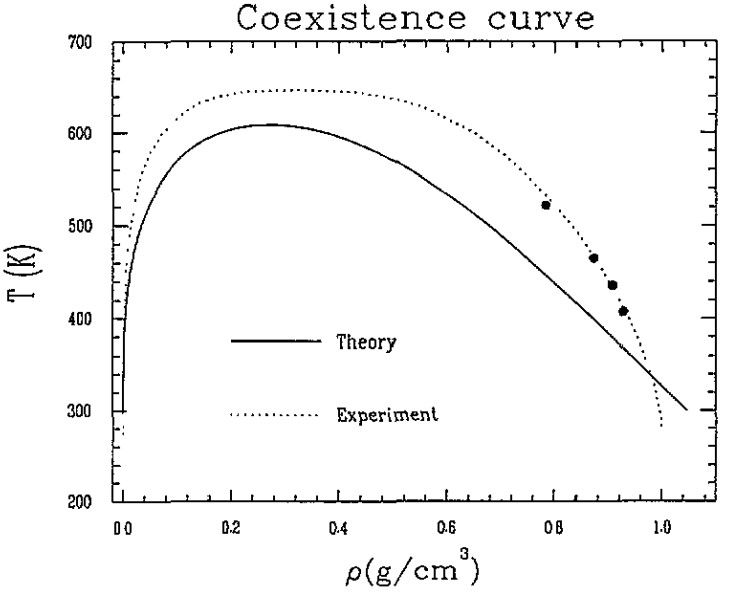

Figure 1. The bulk liquid–vapour coexistence curve for water, comparing present theory with experiment [24]. The points are computer simulation results for the TIP4P model [25].

We next show, in figure 2, the variation of liquid–vapour surface tension γ with temperature. Three 'generations' of the theory are displayed, the highest curve being that obtained previously in [8], which ceased to be valid below 430 K. The next lower curve shows γ obtained from the present theory, but using a hard-sphere repulsive core with fixed diameter $\sigma = 2.95$ Å, the value used in [8]. The third curve contains the results of the present theory using the soft LJ core of the TIP4P model. Softening the core is seen to produce a significant lowering of the surface tension. The lowest curve shows the experimental data [26]. Although our present results for γ are still considerably higher than experiment, they compare more reasonably with the result of MD simulation [15], indicated on the graph, which is only available at the single temperature $T = 325$ K. At this temperature, γ(theory) = 170 dyn cm^{-1}, γ(MD) = 149 ± 18 dyn cm^{-1}, γ(expt) = 68 dyn cm^{-1}.

Calculated density profiles (oxygen-centred) at several temperatures are shown in figure 3. At the lowest temperature, $T = 300$ K, the '10–90' width of the profile has a value $t = 5.75$ Å. This is comparable with but slightly larger than computer simulation

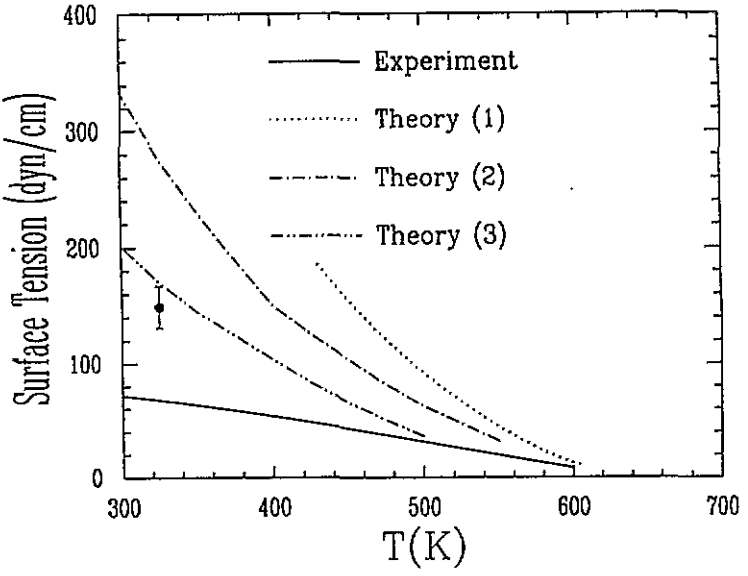

Figure 2. The variation of liquid–vapour surface tension γ with temperature. The three curves labelled (1), (2), (3) correspond, respectively, to the theory of [8], the present theory using a fixed-diameter hard core, and the present theory with the soft repulsive core of the TIP4P model. The single point with its associated error bar is the molecular-dynamics result from [15].

results $t = 5.148$ Å from [27] and $t = 4.70$ Å from [28]. We shall refer back to this figure in discussing next the variation of orientational ordering through the interface. Note that here and in the following figures, distance z is scaled by the Lennard-Jones diameter of the TIP4P model, $\sigma = 3.15$ Å.

Plots of the full angular distribution function $f(z, \theta, \chi)$ against θ and χ for several values of z, at $T = 325$ K, are given in figure 4. Figures 4(a) and (b) show the distribution function at $z/\sigma = -1$ and -0.5, respectively, both lying on the high-density side of the interface (see figure 3). In both of these cases, the distribution function is strongly peaked at polar angle $\theta = 90°$, corresponding to a preferred alignment of dipole axes parallel to the interface. A weak asymmetry in the distribution on reflection about $\theta = 90°$ is present, such that angles $\theta > 90°$ are slightly favoured, which is responsible for a weak net polarization of the interface (discussed further below and in [8]). There is a weak variation of $f(z, \theta, \chi)$ with the dihedral angle χ. At $z/\sigma = -1$, this has maxima at $\chi = 0°$ and 180° (both equivalent by symmetry), corresponding to preferred orientation of the HOH plane perpendicular to the interface. At $z/\sigma = -0.5$, this has changed to produce a weak maximum at $\chi = 90°$, corresponding to predominant alignment of the HOH plane parallel to the interface, but the weakness of this tendency must be emphasized. As seen in figure 4(c), the distribution has changed considerably near the median of the interface at $z/\sigma = 0$. Now three maxima are present, two of which (equivalent by symmetry) occur at $\theta \simeq 52°$, $\chi = 0°$ and 180°. Since the HOH bond angle of the TIP4P model is 104.52°, these maxima can be clearly ascribed to molecular orientations with one OH bond pointing vertically toward the vapour phase. The other maximum in figure 4(c) occurs at $\theta \simeq 116°$, $\chi = 90°$, consistent with a uniform tilt of the HOH plane toward the liquid phase. Bimodel distributions consistent with that of figure 4(c) have been indicated, albeit

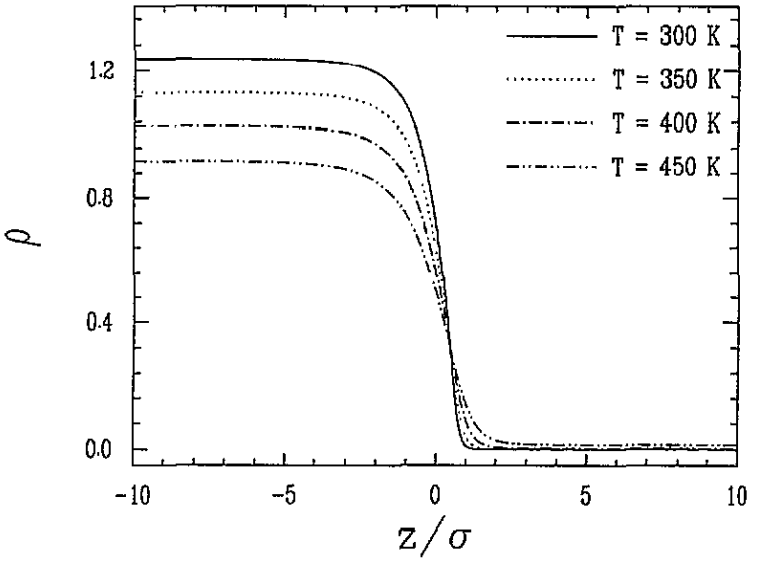

Figure 3. Profile of the number density (oxygen-centred) at several temperatures. The density ρ is given in units of σ^{-3}, where $\sigma = 3.15$ Å is the Lennard-Jones diameter of the TIP4P model.

less definitively, by MD simulations [15,27]. Finally, figure 4(d) shows that $f(z, \theta, \chi)$ undergoes a further dramatic change at $z/\sigma = 0.5$, approaching the vapour side of the interface. Now the maxima in the polar-angle distribution occur at $\theta = 0°$ and 180°, the latter dominating slightly, which indicates a preferred perpendicular alignment of molecular dipoles with a weak bias in favour of dipoles pointing toward the bulk liquid.

The preceding results show that there is a variation of dipole orientation across the interface, from predominantly parallel near the liquid side to perpendicular on the vapour side. This can also be seen from the behaviour of the reduced distribution function of the polar axes

$$P_\mu(z, \theta) = 2\pi \int_0^{2\pi} \mathrm{d}\chi \, f(z, \theta, \chi) \tag{28}$$

which is plotted against z and θ in figure 5, at $T = 325$ K. For $z < 0$, $P_\mu(z, \theta)$ has a maximum at $\theta = 90°$, while at $z > 0$, there are maxima at $\theta = 0°$ and $\theta = 180°$, the latter slightly more pronounced. These results concerning the dipole orientations agree with our previous work [8] and with related density-functional theories [7, 10, 11] for pure dipolar fluids, although with the exception of [28], MD simulations of the water liquid–vapour interface indicate that parallel alignment of dipoles remains dominant at all positions in the interface [15, 27, 29].

The polarization of the interface, resulting from the *weak* asymmetry in the orientational distribution function on reflection about $\theta = 90°$, is shown by the order parameter $\eta_{10} \equiv \langle \cos\theta \rangle$, where $\langle\ \rangle$ denotes angle averaging weighted by $f(z, \omega)$. The profile of this order parameter through the interface exhibits a single negative peak similar to that found in [8], which we omit displaying here. For comparison with the MD simulations of Wilson *et al* [15] on the TIP4P model, we have evaluated a related quantity, namely the

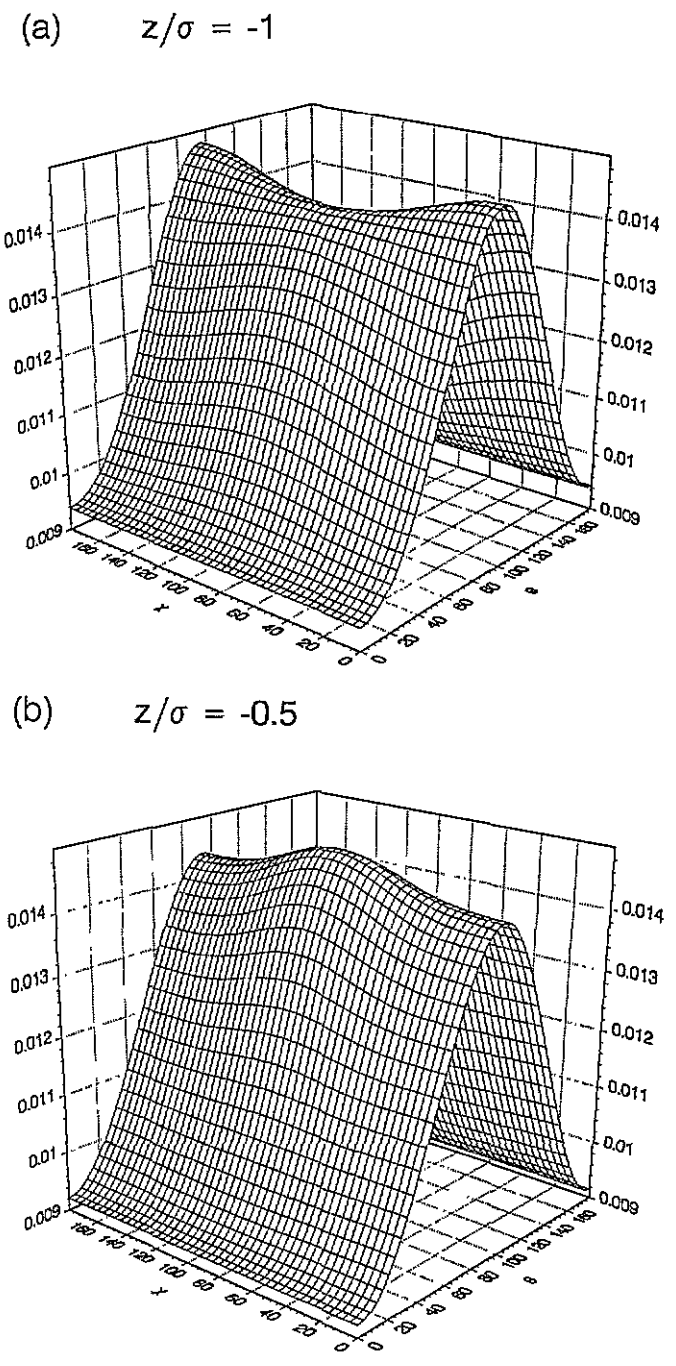

Figure 4. The full angular distribution function $f(z, \theta, \chi)$ against θ and χ for several values of z, at $T = 325$ K.

average z-component of the dipole moment in a thin layer parallel to the interface. This is defined by

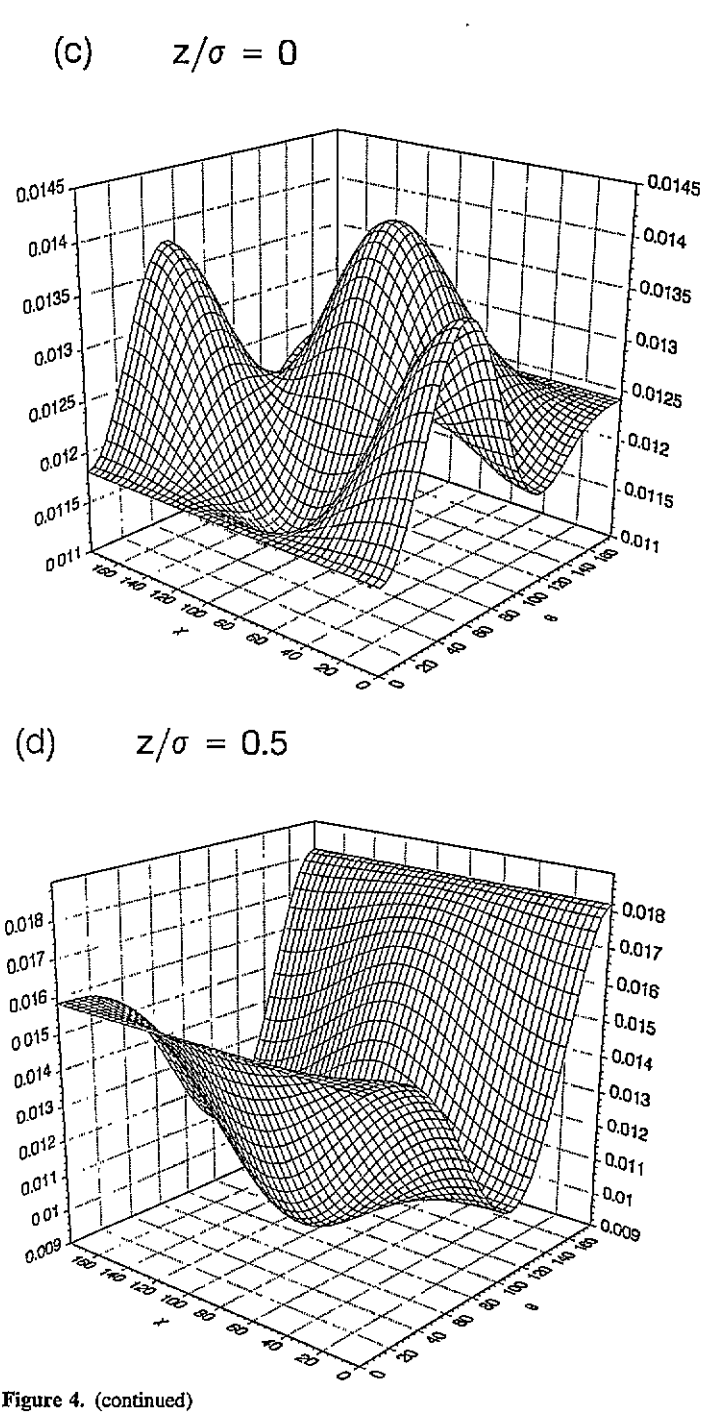

Figure 4. (continued)

$$\bar{\mu}_z = A\mu \int_{z-\Delta z/2}^{z+\Delta z/2} \mathrm{d}z'\, \rho(z')\eta_{10}(z') \tag{29}$$

where μ is the magnitude of the molecular dipole moment, A is the area of the interface,

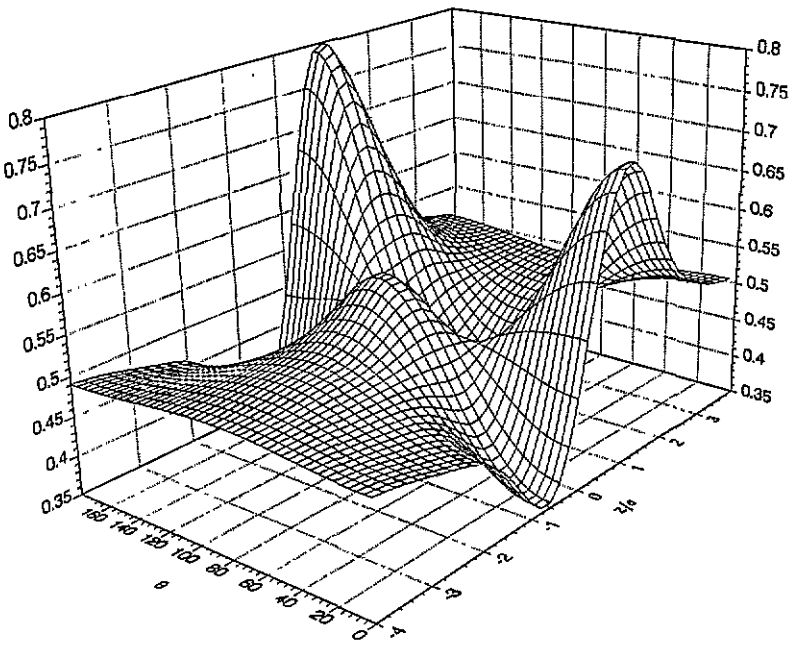

Figure 5. Probability distribution function $P_\mu(z, \theta)$ of dipole orientation against z and θ at $T = 325$ K.

and Δz is the thickness of the layer which is centred at position z. The number density is included in the integrand to count the total molecular population of the layer. We have evaluated (29) from the present theory at intervals of width $\Delta z = 15$ Å, for area $A = (21.71\ \text{Å})^2$, consistent with values used in [15]. The results are shown in figure 6 along with those from [15], where the lines joining the discrete points are merely to guide the eye. For the the sake of comparison, the two sets of data for $\bar{\mu}_z/\mu$ are plotted on different vertical scales. We see that there is very good agreement in the *shape* of the function $\bar{\mu}_z$ against z, but the actual values of the dipole moment differ by one order of magnitude. This indicates that the theory may considerably underestimate the degree of orientational ordering in the interface, to be discussed further in section 4.

The multimodal angular distribution shown by the preceding results begs the question, 'what is the overall preferred orientation of water molecules in the interface?'. This can be answered by counting the numbers of molecules which occur in given orientations over the whole width of the interface. To this end, we divide the full angular intervals for θ and χ into segments of width $\Delta\theta$ and $\Delta\chi$, whose midpoints are denoted θ_m and χ_m, and evaluate the quantity

$$\Delta N(\theta_m, \chi_m) = 2\pi \int_{\theta_m-\Delta\theta/2}^{\theta_m+\Delta\theta/2} \sin\theta \, d\theta \int_{\chi_m-\Delta\chi/2}^{\chi_m+\Delta\chi/2} d\chi \int_{-\infty}^{\infty} dz\, \rho(z)(f(z, \theta, \chi) - 1/8\pi^2). \quad (30)$$

This is interpreted as the total number of molecules per unit area with orientations in the range $\Delta\theta$ and $\Delta\chi$ about θ_m and χ_m, in *excess* of that obtained from a random distribution of molecular orientations for which $f(z, \omega) = 1/8\pi^2$. The subtraction of the latter isotropic distribution, leading to the interpretation of $\Delta N(\theta_m, \chi_m)$ as a surface excess quantity, allows

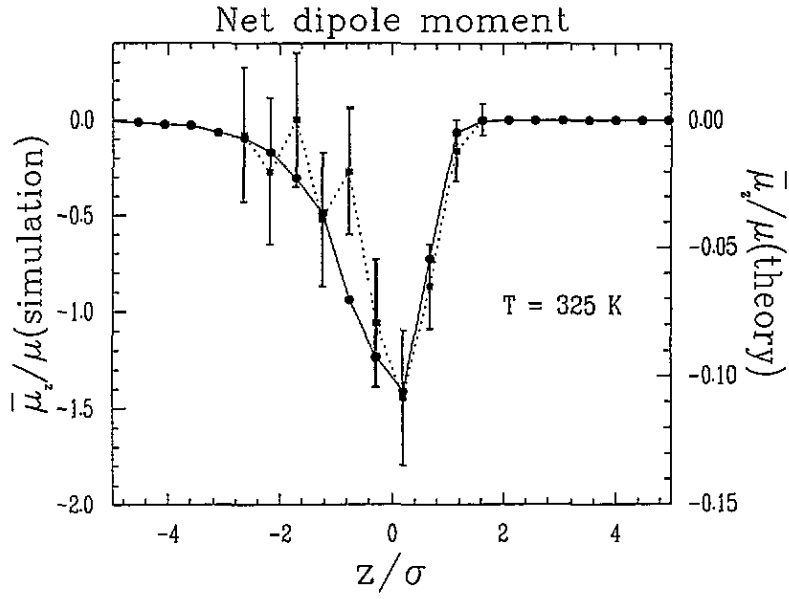

Figure 6. Normalized average net dipole moment in thin interfacial layers, $\bar{\mu}_z/\mu$, as defined in (29). The solid circles (●) and squares (■) are the results of the present theory and the molecular-dynamics simulations [15], respectively.

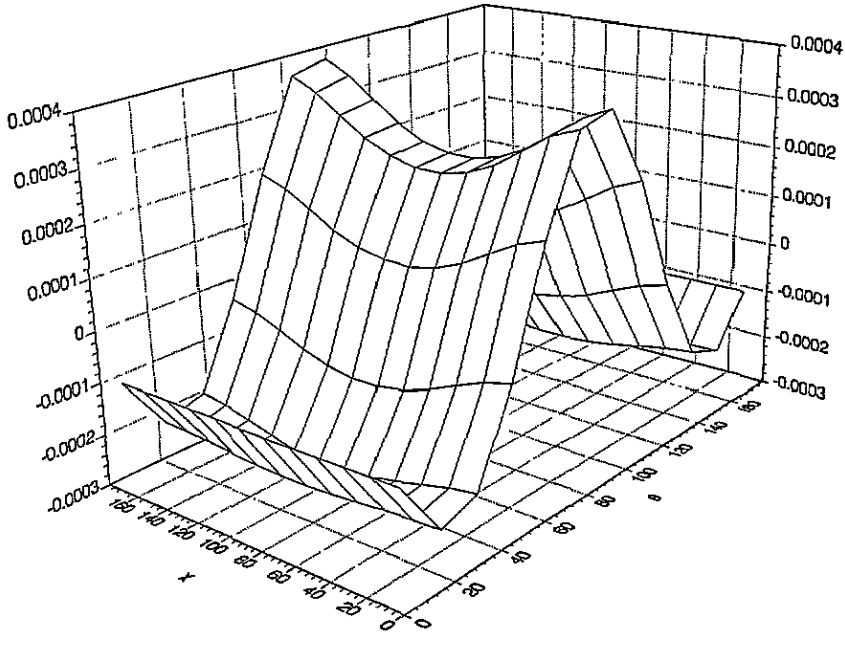

Figure 7. Surface excess angular distribution $\Delta N(\theta, \chi)$ as defined in (30), at $T = 325$ K. The units of ΔN are σ^{-2}.

the z-integration in (30) to be without limits and thus eliminates questions about defining the 'width' of the interfacial zone. For the same reason as in (29), the integration over z is weighted by the number density $\rho(z)$. For the choice $\Delta\theta = \Delta\chi = 15°$, the results for $\Delta N(\theta_m, \chi_m)$ are given on a three-dimensional plot in figure 7, where the continuous lines connect the values at the discrete points (θ_m, χ_m). Not surprisingly, this very clearly shows that the predominant orientation is $\theta = 90°$, $\chi = 0°(180°)$, corresponding to the most probable orientation on the *liquid side* of the interface seen earlier in figure 4(a).

The last quantity we shall examine is the probability distribution of OH bond orientations at the interface. The reduced distribution function $P_{OH}(z, \theta_{OH})$ of the angle θ_{OH} between a molecular OH bond and the positive z-axis is obtained from the full angular distribution $f(z, \omega)$ in the manner described in [8]. Figure 8 shows $P_{OH}(z, \theta_{OH})$ at $T = 325$ K, revealing a multimodal structure somewhat similar to that of $P_\mu(z, \theta)$. In particular, sharp peaks occur at $\theta_{OH} = 0°$ and 180° on the vapour side of the interface. On the liquid side, weak maxima occur at $\theta_{OH} = 180°$ and $\theta_{OH} \simeq 60°$, while the middle region of the interface ($z \simeq 0$) shows maxima at $\theta_{OH} = 0°$ and on a shoulder at $\theta_{OH} < 180°$ of the vapour peak at $\theta_{OH} = 180°$. The positions of these peaks, especially those on the more significant high-density side of the interface, have no obvious relation to those in the full probability distribution shown in figure 4. The maximum in $f(z, \omega)$ at $\theta = 90°$, $\chi = 0°(180°)$ would be expected, naively, to produce $P_{OH}(z, \theta_{OH})$ maxima at $\theta_{OH} \simeq 90° \pm 52°$, whereas the latter are not found. This is related to the weak χ-dependence of $f(z, \omega)$ on the liquid side, which leads to a broad and flat OH bond distribution function. Test calculations on several hypothetical probability distributions show that sharp peaks in $P_{OH}(z, \theta)$ are found only for angular configurations which align either the dipolar axis or an OH bond parallel or antiparallel to the z-axis, structures which are predominant only on the vapour side of the interface.

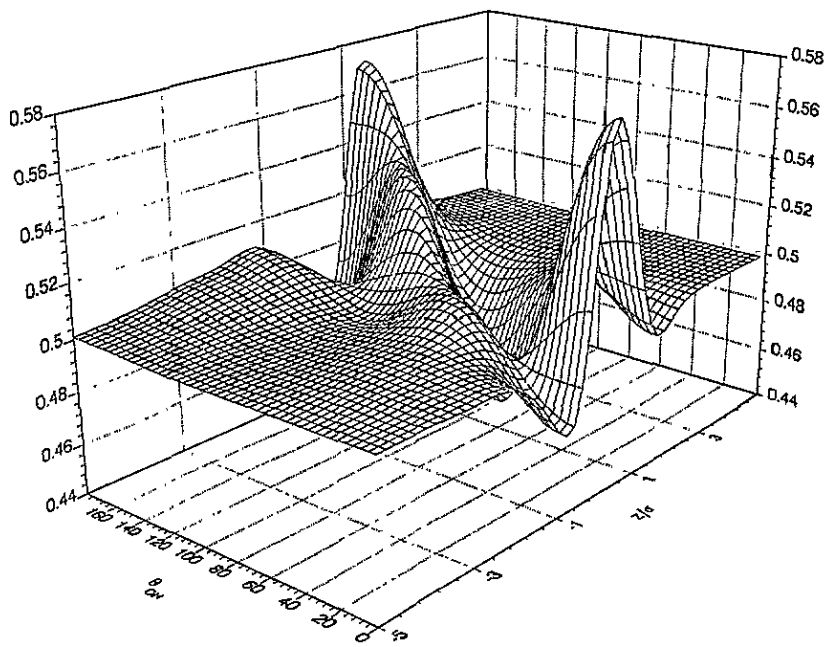

Figure 8. OH-bond orientation distribution function $P_{OH}(z, \theta_{OH})$ against z and θ_{OH} at $T = 325$ K.

The net excess density of OH bond orientations integrated over the interface is defined similarly to (30)

$$\Delta N_{OH}(\theta_{OH}) = \int_{\theta_{OH}-\Delta\theta/2}^{\theta_{OH}+\Delta\theta/2} \sin\theta \, d\theta \int_{-\infty}^{\infty} dz \, \rho(z)[P_{OH}(z,\theta) - \tfrac{1}{2}]. \tag{31}$$

This is shown in figure 9 for $T = 325$ K, indicating that the predominant alignment of OH bonds (after subtracting the random bias) is at $\theta_{OH} \simeq 140°$, i.e., tilted toward the liquid phase. The figure also reveals that OH bonds with $\theta_{OH} < 90°$, i.e., projecting toward the vapour phase, occur with *less* probability than for a random distribution of molecular orientations. If the surface density of 'free' OH bonds is defined as the total surface density of OH bonds with $\theta_{OH} < 90°$, then we conclude that less than 50% of the interfacial molecules exhibit free OH bonds. This is consistent with a lower bound of 20% free OH bonds estimated from sum-frequency generation in [30]. A more precise theoretical value for the surface fraction of free OH bonds is difficult to obtain, since this is sensitive to the definition of interfacial width.

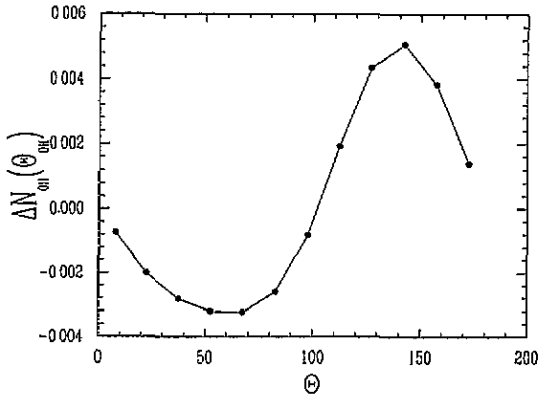

Figure 9. The net excess surface density of OH-bond orientations as defined in (31), at $T = 325$ K. The units of ΔN_{OH} are σ^{-2}.

4. Conclusion

The present work improves upon our earlier theory [8] for the water liquid–vapour interface, enabling us to investigate behaviour near room temperature. The major changes in the theory are the use of the RAM prescription for the effective angle-averaged pair interaction, the consistent treatment of the soft Lennard-Jones core of the TIP4P model pair potential, and use of a high-order multipole expansion of the TIP4P site–site Coulomb potential. These changes, especially the first, require a significantly more complicated numerical analysis of the theory, which we have outlined in section 2. The present theory yields valid results in the entire physical temperature range of liquid water without adjustable parameters.

The predicted dominant surface alignment of water molecules with dipole axes parallel to the surface, accompanied by a weak net polarization pointing from vapour to liquid, agrees

with computer simulation results [15, 27, 29]. We have also found multimodal angular distributions near the median of the interface similar to ones observed in [15, 27], although these are of less statistical weight due to the reduced number density in this region. On the high-density side of the interface, we find a weak preference for orientation of the molecular HOH plane perpendicular to the interface rather than parallel. This is apparently contrary to simulation results [15, 27], but we do not place too much significance on this finding, due to the actual weakness of the variation in dihedral-angle probability. We note that, in the case of [15], the preferred orientations in the interface were deduced primarily from the behaviour of the OH bond distribution function $P_{OH}(z, \theta_{OH})$. At the liquid–vapour interface, however, we have indicated that the interpretation of maxima in $P_{OH}(z, \theta_{OH})$ is highly ambiguous.

The pronounced tendency for perpendicular alignment of dipoles found in section 3 on the vapour side of the interface is also in disagreement with simulation results, although the large statistical uncertainties in simulation data in this region should not be overlooked [28]. The change in preferred dipole orientation from planar to perpendicular on passing from the liquid to the vapour side of the interface can be explained by a simple model of point multipoles in a dielectric continuum with a step-function dielectric profile [11, 31]. While this model is highly idealized, it is physically compelling and gives results in qualitative agreement with the present calculations, where the approximations of the model are absent.

The major discrepancy with computer simulation findings is in the predicted degree of orientational ordering at the interface. This is most clearly shown by the comparison of theory and simulation [15] for the layer dipole moments in figure 6. A weaker indication that the theory underestimates the degree of orientation ordering is the fact that the predicted value for surface tension at 325 K exceeds the simulation result, see figure 2, since increased surface ordering is generally expected to lower the surface tension, although this effect may be masked by those due to other factors such as the difference in bulk densities and the width of the interface [7, 11]. This deficiency of the theory is plausibly linked to the two major approximations involved, namely use of the RAM formula (8) to obtain the effective angle-averaged potential $\bar{V}_{pert}(r_1, r_2)$ and replacement of the reference pair correlation function $g_{ref}(r_1, r_2)$ by its low-density limit (13). Therefore further study to refine these distinct approximations is desirable, for example by approaches described in [21] and [32], respectively.

Even with such refinements of the density-functional theory, it would still be essentially of mean-field character and thus would neglect one other important effect, namely the occurrence of long-wavelength capillary-wave fluctuations, which lead to roughening of the interface [33, 34]. The importance of this effect with respect to the *density profile* of the water liquid–vapour interface has been demonstrated by x-ray reflectivity studies, which indicate that the measured reflectivity can be accurately represented by considering *only* capillary-wave fluctuations [35]. Concerning orientational ordering at interfaces, capillary-wave fluctuations should produce a broadening of the order parameter profiles similar to that of the density profile. This follows from the conventional picture [33, 34] that all short-wavelength fluctuations yield 'intrinsic' profiles which are functions of the distance $z - \xi(x, y)$ from a dividing surface of variable height $\xi(x, y)$, the true profiles being then obtained by averaging over the latter height fluctuations [36]. While the consequences of these fluctuations for comparing theory with experimental results on orientational structure have not (to our knowledge) been addressed, we do not believe this is a serious issue in making comparisons with available computer simulation results, since capillary-wave fluctuations are strongly suppressed by the finite system sizes used in these simulations. From the formula for the mean-square height fluctuation $\langle \xi^2(x, y) \rangle$ of an interface with

linear dimension L, and assuming a microscopic distance cut-off equal to the molecular diameter σ [33, 34], we estimate that the capillary-wave contribution to the interfacial width only becomes comparable to the 'intrinsic' width $t \simeq 5$ Å(see section 3) when $L \gtrsim 200$ Å. This is between six and ten times larger than dimensions used in recent simulations of the water surface [15, 27, 28], requiring of the order of 3×10^5 molecules, sizes which may soon be attainable with modern computer technology.

Acknowledgment

We gratefully acknowledge the financial support of the Natural Sciences and Engineering Research Council of Canada (NSERC).

References

[1] Evans R 1992 *Fundamentals of Inhomogeneous Fluids* ed D Henderson (New York: Dekker) ch 3
[2] Telo da Gama M M 1984 *Mol. Phys.* **52** 858, 611
Telo da Gama M M and Thurtell J H 1986 *J. Chem. Soc. Faraday Trans.* II **82** 1721
[3] Tjipto-Margo B, Sen A K, Mederos L and Sullivan D E 1989 *Mol. Phys.* **67** 601
Mederos L and Sullivan D E 1992 *Phys. Rev.* A **46** 7700
[4] Moore B G and McMullen W E 1992 *J. Phys. C: Solid State Phys.* **96** 3374
[5] Telo da Gama M M and Gubbins K E 1986 *Mol. Phys.* **59** 227
Telo da Gama M M and Sebrosa J M 1992 *Dynamical Phenomena at Interfaces, Surfaces, and Membranes* ed D Beysens *et al* (New York: Nova Science)
[6] Somoza A M and Desai R C 1992 *J. Phys. C: Solid State Phys.* **96** 1401
[7] Teixeira P J and Telo da Gama M M 1991 *J. Phys.: Condens. Matter* **3** 111
[8] Yang B, Sullivan D E, Tjipto-Margo B and Gray C G 1992 *Mol. Phys.* **76** 709
[9] Yang B, Sullivan D E, Tjipto-Margo B and Gray C G 1991 *J. Phys.: Condens. Matter* **3** 109
[10] Frodl P and Dietrich S 1992 *Phys. Rev.* A **45** 7330
[11] Frodl P and Dietrich S 1993 *Phys. Rev.* E **48** 3741
[12] Cherepanova T A and Stekolnikov A V 1991 *J. Chem. Phys.* **154** 41
[13] Rickayzen G 1992 *Mol. Phys.* **75** 333
[14] Jorgensen W L, Chandrasekhar J, Madura I D, Impey R W and Klein M L 1983 *J. Chem. Phys.* **79** 926
[15] Wilson M A Pohorille A and Pratt L R 1987 *J. Phys. C: Solid State Phys.* **91** 4873; 1988 *J. Chem. Phys.* **88** 3281; 1989 *J. Chem. Phys.* **90** 5211
[16] Smith W R 1974 *Can. J. Phys.* **52** 2022
Perram J W and White L R 1974 *Mol. Phys.* **28** 527
[17] Gray C G and Gubbins K E 1984 *Theory of Molecular Fluids* (Oxford: Clarendon)
[18] Williams G O, Lebowitz J L and Percus J K 1984 *J. Chem. Phys.* **81** 2070
[19] Tjipto-Margo B and Sullivan D E 1988 *J. Chem. Phys.* **88** 6620
[20] Woodward C E and Nordholm S 1984 *Mol. Phys.* **52** 973
[21] Woodward C E and Nordholm S 1986 *Mol. Phys.* **59** 1177; 1987 *Mol. Phys.* **60** 415
[22] Weeks J D, Chandler D and Andersen H C 1971 *J. Chem. Phys.* **54** 5237
[23] Fries P H and Patey G N 1986 *J. Chem. Phys.* **85** 7307
[24] Haar L, Gallagher J S, Kell G S 9184 *NBS/NRC Steam Tables: Thermodynamic and Transport Properties and Computer Programs for Vapor and Liquid States of Water in SI Units* (New York: McGraw-Hill)
[25] de Pablo J J and Prausnitz J M 1989 *Fluid Phase Equilibria* **53** 177
[26] Floriano M A and Angell C A 1990 *J. Phys. C: Solid State Phys.* **94** 4199
[27] Matsumoto M and Kataoka Y 1988 *J. Chem. Phys.* **88** 3323
[28] Lie G C, Grigoras S, Dang L X, Yang D-Y and McLean A D 1993 *J. Chem. Phys.* **99** 3933
[29] Townsend R M and Rice S A 1991 *J. Chem. Phys.* **94** 2207
[30] Du Q, Superfine R, Freysz E and Shen Y R 1993 *Phys. Rev. Lett.* **70** 2313
[31] Buff F P and Goel N S 1972 *J. Chem. Phys.* **56** 2405
[32] Mederos L, Navascues G, Tarazona P and Chacon E 1993 *Phys. Rev.* E **47** 4289

[33] Weeks J D 1977 *J. Chem. Phys.* **67** 3106

[34] Gelfand M P and Fisher M E 1990 *Physica* A **166** 1

[35] Schwartz D K, Schlossman M L, Kawamoto E H, Kellogg G J, Pershan P S and Ocko B M 1990 *Phys. Rev.* A **41** 5687

Pershan P S 1990 *Faraday Discuss. Chem. Soc.* **89** 231

It should be noted, nonetheless, that these studies cannot distinguish between alternative data fittings which assume a non-zero 'intrinsic' contribution to the interface reflectivity.

[36] We neglect any decorrelation between interface normal directions, i.e., 'crumpling' effects (Peliti L and Leibler S 1985 *Phys. Rev. Lett.* **54** 1690), as these effects are suppressed by the non-zero interfacial tension.